Computer Methods and Programs in Biomedicine 269 (2025) 108890



Contents lists available at ScienceDirect

Computer Methods and Programs in Biomedicine

journal homepage: www.sciencedirect.com/journal/computer-methods-and-programs-in-biomedicine





Automated phenotypic analysis and classification of drug-treated cardiomyocytes via synergized time-lapse holographic imaging and deep learning

Ezat Ahmadzadeh, Seonghwan Park, Youhyun Kim, Inkyu Moon *

Department of Robotics & Mechatronics Engineering, Daegu Gyeongbuk Institute of Science & Technology (DGIST), 333 Techno Jungang-daero, Hyeonpung-myeon, Dalseong-gun, Daegu 42988 South Korea

ARTICLE INFO

Keywords:
Time-lapse holographic biosensors
Deep learning-based cardiomyocytes analysis
Cardiac cell classification
Cardiotoxicity screening
Precision medicine systems

ABSTRACT

Background and Objective: Predicting cardiovascular risk is critical for the therapy and control of cardiovascular illnesses. This work studies screening the toxicity of three drugs, (E-4031, isoprenaline, and sertindole) with various concentrations using tracking of the single cardiac cell's contractile motion to explore the drug concentration impact on single cell contractile dynamics and automated classification based on cells motion behavior using deep transfer learning and different machine learning based methods.

Methods: We developed an integrated platform for automated dynamic analysis and classification of human-induced pluripotent stem cell-derived cardiomyocytes (CM) at the single-cell level that uses a combination of holographic image-based tracking and deep learning. For in-depth investigation and automated classification of CMs, first, we accurately extracted a single CM's dry mass using time-lapse holographic imaging and a deep fully convolutional network. Afterward, we applied the Farneback optical flow method to track the cell's contractile motion frame by frame through the extracted single CMs with single-pixel displacement detection. Following this, a computational algorithm was developed to further characterize the single CM's functional behaviors, and several beating activities–related parameters were calculated. The average result of the population for every measured parameter was compared to the control condition using an unpaired student *t*-test. Finally, we proposed a fine-tuned deep transfer learning-based model for automated cell classification based on the compound's mode of action from the single-cell motion waveform and compared the result to feature-based single-cell classification using different machine learning approaches. We also provided reliable synchronization analysis of drug-treated CMs owing to cellular analysis at the single-cell level.

Results: Cardiomyocytes responded to isoprenaline by speeding up their action potentials, increasing the frequency of their beats. The action potential speed was reduced and the resting time was lengthened in the presence of E-4031 and sertindole lowering the beat frequency. Performance analysis of the deep transfer learning-based model was carried out using several well-known evaluation metrics. A performance analysis shows the proposed model achieved 98.8 % classification accuracy.

Conclusions: Our implementation allowed precise single drug-treated CM motion tracking and in-depth investigation and automated classification of CMs via synergized time-lapse holographic imaging and deep learning.

1. Introduction

Digital holographic microscopy (DHM) can provide accurate quantitative visualization of human cardiomyocytes derived from human-induced pluripotent stem cell (hiPSC) dynamics, which are transparent or semi-transparent microscopic objects [1–8]. As a result, significantly valuable information regarding cell dynamics of dry mass redistribution can be obtained in a label-free manner [9]. Human cardiomyocyte cells pump blood to the entire body with synchronized beating activity [10]. HiPSC technology was shown to be an alternative model for in vitro cardiotoxicity screening in new-compound human disease modeling, cardiotoxicity testing, and therapy in vitro [11,12]. Drugs that cause cardiac arrhythmia cause alterations in CM physiological behaviors (dry mass redistribution), such as changes in contraction–relaxation

* Corresponding author.
E-mail address: inkyu.moon@dgist.ac.kr (I. Moon).

https://doi.org/10.1016/j.cmpb.2025.108890
Received 6 May 2023; Received in revised form 23 January 2025; Accepted 1 June 2025
Available online 4 June 2025
0169-2607/© 2025 Elsevier B.V. All rights are reserved, including those for text and data mining, AI training, and similar technologies.

motion–speed, beating frequency, contraction period, relaxation period, and motion patterns. Therefore, high-throughput preclinical cardio-safety assessment methods for CM characterization in cardiotoxic screening are in crucial demand. Many authors have reported methods for CM characterization, including patch clamping [13,14], calcium imaging [15,16], and image processing–based contraction–relaxation studies [17,18]. All the above-mentioned methods require expensive equipment or specific expertise, which demonstrates the shortcomings in simplified methods for CM motion characterization at the single-cell level analysis.

Optical flow-based real-time motion characterization offers low-cost and high-throughput methods capable of monitoring CM contractile activity without physical contact, which maintains the sample's paradigm [19–23]. The Farneback dense optical flow method performs tracking by measuring the displacement of each pixel in an image suitable for CM contractile kinetic analysis at the single-cell level. However, accurate CM's dry mass extraction from the quantitative phase images (QPIs) is a challenging task due to the variations in shape, size, orientation, and lack of special geometry. A fully convolutional network (FCN) is a promising tool for single-CM dry mass extraction from QPIs using the pixel classification technique [25–28]. In a recent study, we reported an FCN-based method to extract the nucleus parts from QPIs for single-CM functional behavior characterization based on simple image processing [29].

In the current study, we present a highly accurate and fully automated method for characterizing single-CM kinetics by combining optical flow and deep learning-based phase image segmentation. The dry mass of seven single CMs was automatically extracted under control and drug-treated conditions using the FCN model. Afterward, the Farneback optical flow method with single-pixel displacement detection was applied to monitor the dynamic, rhythmic beating patterns, and a contractile motion waveform was generated. Following this, a computational algorithm was implemented to characterize the contractile motion of single cardiomyocytes from the motion waveform signal, and multiple parameters related to the periodicity of the CM beating activity profile were measured such as contraction motion–speed, relaxation motion–speed, contraction period, relaxation period, and resting period, and their standard deviations. We demonstrated the robustness of the proposed algorithms by comparison with other optical flow methods for CM motion tracking and analysis. In addition, the extracted features were used for feature-based single-cell classification using machine learning approaches. Furthermore, we screened the toxicity of three drugs, (E-4031, isoprenaline, and sertindole) with various concentrations at the single-cell level. Our results demonstrated that the E-4031 compound reduces the contraction–relaxation motion–speed, compared to the control, while isoprenaline increases the contraction–relaxation motion–speed. Sertindole causes an increase in contraction motion–-speed while the relaxation motion–speed is reduced, compared to the control. We also provided reliable synchronization analysis of drug-treated CMs owing to cellular analysis at the single-cell level. Finally, we propose a fine-tuned deep transfer learning-based model for automated drug type classification from the single-cell motion waveform. A performance analysis shows the proposed model achieved 98.8 % classification accuracy based on the drug mode of action from single cells motion waveform.

2. Material and methods

2.1. Digital holographic imaging

Off-axis digital holographic microscopy (DHM) was employed to produce CMs' phase images. Steps of cardiac cell imaging using an off-axis DHM are shown in the Supplementary Figure S1 [30,31]. In Supplementary Section 1, we go through how holographic image is created in further depth.

2.2. Cardiomyocyte cell preparation

Human-induced pluripotent stem cell-derived CMs (iCell cardiomyocytes, CMC-100–010–001) obtained from Cellular Dynamics Int. (Madison, WI) were cultured and grown according to the manufacturer's instructions for 14 days before recording a hologram of CMs. Measurements were acquired in a Chamlide WP incubator system with a 96-well plate (LCI, South Korea) set at 37°/5 % CO_2 with high humidity. Cardiomyocyte images were obtained using a Leica 20 × /0.4 NA objective. The QPIs of cardiomyocytes were acquired at a 50 Hz sampling frequency for 30 s. For the control condition, a sequence of QPIs was recorded before treatment. Following this, the drugs were added at different concentrations in individual wells. Experiments were conducted in triplicate (three separate wells with one 330 × 330 μm field acquired per well containing about 50 cells).

2.3. Cardiac cell fixation

Cardiomyocytes were fixed in a 4 % formalin solution (Sigma-Aldrich) and incubated at room temperature for 15 min (RT). Following that, cells were washed three times with phosphate-buffered saline (PBS) for 10 min at room temperature. Before and after cell fixation, 1500 pictures were taken at a sampling frequency of 50 Hz.

2.4. Preprocessing

The median filter is a widely used method to remove noise from an image or signal. In this experiment, we applied a 3D median filter with a window size of 2 × 2 × 2 for noise reduction. This specific window size was chosen based on the previous works [24,32], which proposed it as a practical approach for the automated quantification of drug-treated cardiomyocytes.

2.5. Cardiac cell–motion tracking with farneback optical flow

The Farneback method uses polynomial expansion in multi-resolution levels for displacement estimation. In the first step, the algorithm generates multi-resolution levels from the original image using Gaussian pyramids, where each level has a lower resolution than the previous level. The tracking process starts with the lowest resolution and continues to the highest resolution. Consequently, the displacement of two local patches in consecutive image frames is calculated using the following equation [33]:

$$I(\mathbf{x}) \approx \mathbf{x}^T\mathbf{A}\mathbf{x} + \mathbf{b}^T\mathbf{x} + c, \tag{1}$$

where $\mathbf{A}$ stands for symmetric matrix, $\mathbf{b}$ is a vector, and c is a scalar. The vector $\mathbf{x}$ is a 2 × 1 vector. The first neighborhood is approximated with the following equation:

$$I_1(\mathbf{x}) = \mathbf{x}^T\mathbf{A}_1\mathbf{x} + \mathbf{b}_1{}^T\mathbf{x} + c. \tag{2}$$

The displacement of the neighborhood is considered via vector $\mathbf{d}$. The new neighborhood, affected by displacement $\mathbf{d}$, is calculated as follows:

$$\begin{aligned} I_2(\mathbf{x}) &= I_1(\mathbf{x}-\mathbf{d}) = (\mathbf{x}-\mathbf{d})^T\mathbf{A}_1(\mathbf{x}-\mathbf{d}) + \mathbf{b}_1^T(\mathbf{x}-\mathbf{d}) + c_1 \\ &= \mathbf{x}^T\mathbf{A}_1\mathbf{x} + (\mathbf{b}_1 - 2\mathbf{A}_1\mathbf{d})^T\mathbf{x} + \mathbf{d}^T\mathbf{A}_1\mathbf{d} - \mathbf{b}_1^T\mathbf{d} + c_1 \ = \mathbf{x}^T\mathbf{A}_2\mathbf{x} + \mathbf{b}_2^T\mathbf{x} + c_2. \end{aligned} \tag{3}$$

Using different coefficients from two polynomials, $I_2(\mathbf{x})$ and $I_1(\mathbf{x}–\mathbf{d})$, gives $\mathbf{A}_2$=$\mathbf{A}_1$, $\mathbf{b}_2$=$\mathbf{b}_1$–2$\mathbf{A}_1\mathbf{d}$, and c_2=$\mathbf{d}^T\mathbf{A}_1\mathbf{d}$–$\mathbf{b}_1^T\mathbf{d}$+$c_1$. The displacement, $\mathbf{d}$, which is used to approximate the optical flow, is obtained with the following equation:

$$\mathbf{d} = -\frac{1}{2}\mathbf{A}_1^{-1}(\mathbf{b}_2 - \mathbf{b}_1). \tag{4}$$

Tracking initializes from the lowest resolution level and finishes at

the highest. The detected tracking points at each level are considered the starting point for the next level. By using multi-resolution–level tracking, a large displacement can be detected (see Supplementary Fig. S2).

2.6. Single-CM dry mass extraction using a fully convolutional network

The extraction of dry mass is critical for accurate, label-free quantification of cardiomyocyte physiological behaviors. Dry mass serves as a surrogate marker for understanding cellular health and activity, as it reflects the redistribution of intracellular components during contraction and relaxation. This parameter provides unique insights into CM motion dynamics and mass redistribution, which are not accessible through conventional imaging or electrophysiological methods. By isolating the dry mass, we ensure precise single-cell level analysis, enabling reliable measurements of contractile behavior under drug-treated and control conditions. To achieve this, we utilized a fully convolutional network for dry mass extraction from quantitative phase images. The extracted dry mass was then integrated into the workflow to assess motion characteristics of single CMs.

Convolutional neural network (CNN) mainly consists of the following elements: 1) a set of learnable filters to extract local features; 2) a nonlinear function as an activation function; 3) a max-pooling layer that aggregates the local feature specification to reduce data dimensions. Details of the proposed FCN structure's elements were explained in our previous study [29]. For better network performance in cardiac image feature extraction, we used parallel multi-pathway feature concatenation (see Fig. 1(b)). In this technique, different feature maps extracted by various kernel sizes are concatenated. We propose using different kernel sizes in different pathways in parallel (1×1, 3×3, and 5×5) to concatenate different feature types, followed by batch normalization (BN) and a rectified linear unit (ReLU).

2.7. Workflow and cardiomyocyte contractile response parameter assessment

We extracted seven single CMs from different parts of a whole-slide QPI from multiple CMs. See Fig. 1(a). The QPIs with multiple CMs had a resolution of 800×800 pixels (224 μm). The motion waveform was generated from a CM's motion–speed calculation during spontaneous contraction–relaxation beating activity by using the following equation:

$$Speed_{\mu m/s} = \left|\frac{Displacement}{Time}\right| = \frac{\sqrt{(dx)^2 + (dy)^2}}{Time}, \quad (5)$$

where dx and dy are displacements in x and y directions estimated by the Farneback algorithm, representing CM motion in the x and y directions, and time was considered to be the time between two consecutive image frames [24]. Afterward, we extracted several parameters related to the contractile motion profile including maximum contraction speed, beating period, contraction period, relaxation period, maximum relaxation speed, and resting period.

The overall structure of the FCN model is shown in Fig. 1(b). Afterward, the optical flow method was applied to a single CM image sequence, and contractile motion–speed was calculated as shown in Fig. 1(c). While a cell is in spontaneous contraction–relaxation, the motion vectors overlaid on the image of a single cell indicate the opposite direction (see Figs. 1(d) and (e)). After one beating cycle (contraction–relaxation) the cell enters the resting state in which the motion vectors show no direction. See Fig. 1(f). The overall beating activity profile obtained using motion–speed calculation is shown in Fig. 1(g). Finally, to demonstrate the robustness and accuracy of the single-CM motion tracking approach, we propose a fine-tuned GoogLeNet for automated drug type identification from the single-cell motion waveform shown in Fig. 1(h). The inset shows details of the multiple parameters calculated from the beating activity Fig. 1(i).

It is crucial to use multiple parameters to evaluate the effects of compounds for precise capturing of the irregularity and dynamics of the beating profile. Fig. 1(i) shows a motion waveform of a single CM (generated from the motion–speed calculation), which consists of a sequence of positive peaks for contraction–relaxation, and the contractile motion waveform is quantified through contraction–relaxation peak identification [34]. Different methods have been proposed to find the QRS complex [20,35,36]. Details on accurate peak detection, along with the auxiliary points, were described in our previous study (Ahmadzadeh et al., 2020). For data analysis, the mean and standard deviation (SD) of the related parameters are calculated. The extracted beating activity-related parameters and the corresponding descriptions are explained as follows. 1) Maximum contraction speed (see #1 in Fig. 1(i)): The average amplitude of contraction peaks; 2) Beating period (see #2 in Fig. 1(i)): The time between two adjacent contraction peaks; 3) Contraction period (see #3 in Fig. 1(i)): The average time between the start-of-contraction and end-of-contraction points; 4) Relaxation period (see #4 in Fig. 1(i)): The average time between start-of-relaxation and the end-of-relaxation; 5) Maximum relaxation speed (see #5 in Fig. 1(i)): The average amplitude of relaxation peaks; 6) Resting period (see #6 in Fig. 1 (Inset)) The average time between end-of-relaxation and the next start-of-contraction

2.8. Statistical analysis

An unpaired Student's t-test was used to compare the average results of the population for each measured parameter between control and drug-treated conditions. This test was chosen to determine the statistical significance of differences in means between these independent groups. Data are presented as mean ± standard deviation (SD), and significance levels were reported as follows: ($^*P < 0.05$), ($^{**}P < 0.01$), ($^{***}P < 0.001$), ($^{****}P < 0.0001$).

3. Results

3.1. Whole-slide quantitative phase image (QPI) analysis

We first tested a compound's effect on beat rate frequency changes in the waveforms, comparing control conditions and treated conditions. The beat rate frequency changes were observed in the contractile motion patterns of the whole-slide QPIs of multiple hiPSCs compared to the control condition depending on the compound's mechanism of action. The drug effect on the motion waveform manifests itself by changing the beat rate as a direct consequence (see Supplementary Figs. S3, S4, S5, S6, and S7). The cardiomyocytes responded to isoprenaline with action potential shortening after increases in the drug concentration, thus increasing the beating frequency. A high concentration (500 nM) of isoprenaline markedly increased the beat rate. High concentrations of E-4031 and sertindole similarly demonstrated a reduction in beating frequency where 500 μM of E-4031 and 200 nM of sertindole significantly reduced beating frequency. We quantified three whole-slide QPIs from multiple cardiomyocyte samples under control conditions as a representative of all control conditions, and the corresponding quantification parameters are in Supplementary Table 1.

3.2. Drug effects on contractile motion–speed

We carried out a comparison of contraction motion–speed before and after treatment with a drug. However, the additional parameters were also evaluated to precisely determine the effects of the drugs. We evaluated sertindole, E-4031(HERG channel blocker), and isoprenaline effects on CM motion–speed along with other critical parameters. Sertindole is the second generation of antipsychotic phenylindole-derived medication compounds that function as an antagonist in a portion of receptor systems [37]. The sertindole effect was manifested in prolonged repolarization as a direct consequence. Afterward, we

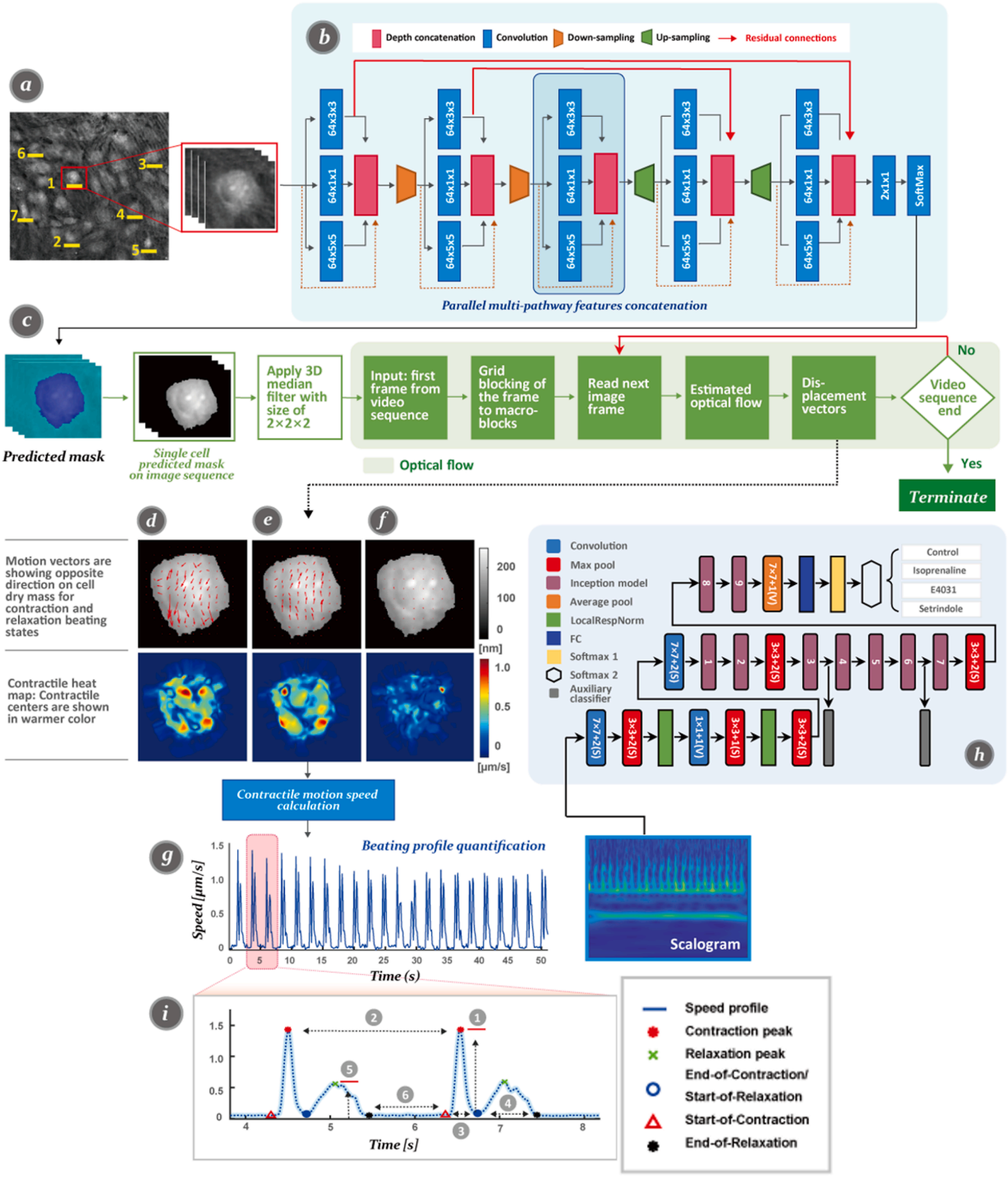


Fig. 1. An overview of the workflow for motion tracking of single cardiac cells and beating profile visualization. (a) A cardiomyocyte phase image after numerical reconstruction with multiple cardiac cells. (b) The proposed FCN model structure for single-CM dry mass extraction. (c) The optical flow procedure for a cardiac cell's contractile motion–speed measurement. In (d), (e), and (f), motion vectors are superimposed on the cell's phase image for contraction–relaxation and resting activities, respectively, and the corresponding heat map generated from absolute motion is shown in the second row (A contractile center, shown in a warmer color on the heat map, indicates a region in which contractions are maximized). (g) The motion–speed beating activity profile of a single CM is generated from the cell's motion–speed measurement (see Supplementary Video 1). (h) The fine-tuned GoogLeNet with an additional layer, optimal parameters, and transferred weights. (i) Inset shows details of the multiple parameters calculated from the beating activity.

investigated the effect of E-4031 on a CM's motion waveform. Treatment of cardiac cells with E-4031 significantly slowed the heart rate and attenuated the loss of intracellular K^+ in cardiac cells [38]. A comparison of the critical parameters under control and drug-treated conditions in the presence of 500 μM of E-4031 showed the contraction period slightly decreased along with prolongation in the relaxation period. The corresponding beating period and resting period were significantly increased, and thus, the beat rate declined. Finally, we carried out a similar experiment to evaluate the effects of isoprenaline. The isoprenaline compound is a beta-1 and beta-2 adrenergic receptor agonist that exerts its effects through a G-alpha stimulatory second messenger system [39]. The isoprenaline compound increased the beat rate frequency while decreasing the overall duration of each beat.

3.3. Quantification at the single-cell level

First, we extracted single CMs using the FCN model, and motion waveforms were generated using the optical flow method. Secondly, the computational algorithm was applied to extract several quantification parameters for every single cell, and a population average was computed for control and drug-treated conditions to represent the motion characteristics in response to each drug concentration. For dry-mass extraction, a total of seven cells were analyzed to ensure a balanced comparison across different drug treatment conditions. In this analysis, a comparable number of samples were selected for each drug concentration, which resulted in the use of a smaller number of control cells. This approach allowed for meaningful cross-condition comparisons while minimizing variability introduced by differences in sample sizes. Since our current analysis captures the drug effects on a discrete population of individual cells, it is plausible that differences in contractile motion–-speed were observed after averaging the population. Since our analyses are at the single-cell level, they can provide reliable synchronization analysis (see Supplementary Fig. S8, S9). GraphPad Prism 8 (GraphPad Software, Inc) was used to conduct statistical analysis to detect significant differences between groups for other critical parameters.

3.3.1. Effects of sertindole treatment

The sertindole effect manifested itself in CMs, showing prolonged repolarization as a direct consequence. Fig. 3 illustrates the quantification of different parameters per cell. Fig. 2(a) shows the contractile motion–speed of the whole-slide QPI in response to 200 nM of sertindole (the single beat is shown) and corresponding quantification results. Fig. 2(a) of the bar chart shows quantification results for whole-slide QPI in response to 200 nM of sertindole compared to the control condition. The whole-slide QPI in response to 200 nM of sertindole demonstrated contraction upstroke motion–speed increased, whereas relaxation motion–speed decreased, compared to the control. Also, alteration of critical parameters was observed, including prolongation in the relaxation period, beating period, and resting period. Fig. 2(c) shows single-cell population analysis in drug-treated versus control conditions. As one can see from Fig. 2(c), sertindole treatment exhibited a significant prolongation in resting time. Fig. 2(d) demonstrates a population average of extracted single cells. In Fig. 2(d), sertindole did not significantly change the contraction period, whereas the resting period and beating intervals were significantly prolonged. There was variation in contractile motion–speed between individual single cells, while a decreasing trend was observed when averaging the population for relaxation motion–speed. The differences in the other critical parameters were evaluated with an unpaired *t*-test.

3.3.2. Effects of isoprenaline treatment

Isoprenaline, increased the beat rate frequency while decreasing the overall duration of each beat. Fig. 3(a) shows the contractile motion waveform of the whole-slide QPI of the hiPSC in control versus drug-treated conditions in response to 500 nM isoprenaline (the single beat is shown) and the corresponding quantification results are shown in Fig. 3(b). As seen in Fig. 3(a), contraction–relaxation motion–speed increased, compared to the control condition, in response to 500 nM of isoprenaline. Fig. 3(c) shows single-cell population analysis in drug-treated versus control conditions. Fig. 3(d) demonstrates a population average of extracted single cells. Fig. 3 shows the contractile motion of individual single cells and the average population under control and drug-treated conditions and in the presence of different concentrations of isoprenaline along with corresponding quantification results. The differences in the other critical parameters were evaluated with an unpaired *t*-test.

3.3.3. Effects of E-4031 treatment

E-4031 decreased contraction and relaxation motion–speed and prolonged the resting period in hiPSCs (depending on the concentration level), which is in line with our previous study (see Fig. 4). Fig. 4(a) shows the contractile motion waveform of the whole-slide QPI of the hiPSC in control versus drug-treated conditions in response to 500 nM E-4031 (the single beat is shown) and the corresponding quantification results, which are shown in Fig. 4(b). Fig. 4(a) shows the contractile motion in a whole-slide QPI of an hiPSC under control and drug-treated conditions in response to 500 μM of E-4031 contraction–relaxation motion–speed declined. However, the degree of change in beating frequency varied significantly between different levels of drug concentration. Fig. 4(c) shows single-cell population analysis in drug-treated versus control conditions where single cells are individually investigated. Fig. 4(d) shows the contractile motion of individual single cells and the average population under control and drug-treated conditions and in the presence of different concentrations of E-4031. The differences in the other critical parameters were evaluated with an unpaired *t*-test.

3.3.4. Verification of the proposed cardiac cells motion tracking method

The procedure was validated by comparing the speed of fixed cardiomyocytes to living cardiomyocytes (See Fig. 5(a)). The amplitude of fixed cell speed swings about zero. The amplitude is substantially less than the contraction-relaxation peaks and similar to the resting state amplitude (see Supplementary Video 5). In addition, the proposed Farneback optical flow was compared against commonly used Lucas-Kanade [40] and Horn–Schunck [41]. optical flow methods for CM motion tracking. The experimental results demonstrated the proposed dense optical flow method can efficiently track the tiny motion of cardiac cells and extract the beating profile of cardiac cells while other optical flow-based models failed to show this result (see Fig. 5(b)).

3.3.5. Feature-based cardiac cell classification using machine learning approaches

We utilized different machine-learning approaches for feature-based drug type categorization using characteristics collected from the motion wave of single cardiac cells. There were 161 single cells utilized in total for machine learning-based categorization. In the control condition, there are 11 single cells, 48 single cells for E-4031, 52 single cells for isoprenaline, and 50 single cells for the Sertindole medication. The smaller number of control single cells reflects the primary focus of this study on analyzing drug-induced changes. The control condition served as a baseline to compare the effects of the drugs, and the available control dataset was sufficient to establish reliable baseline parameters for statistical comparisons. Resource constraints, including the time and cost of generating control datasets, also contributed to this imbalance. To ensure a comprehensive evaluation of the model's performance and avoid potential bias due to small test set sizes, we adopted a 5-fold cross-validation approach for both machine learning and deep learning techniques. In this approach, the dataset was systematically divided into five equal parts, with each subset used as a test set once while the remaining subsets were used for training. This procedure ensures that the entire dataset is used effectively for both training and testing at different stages, with an effective split of 80 % for training and 20 % for

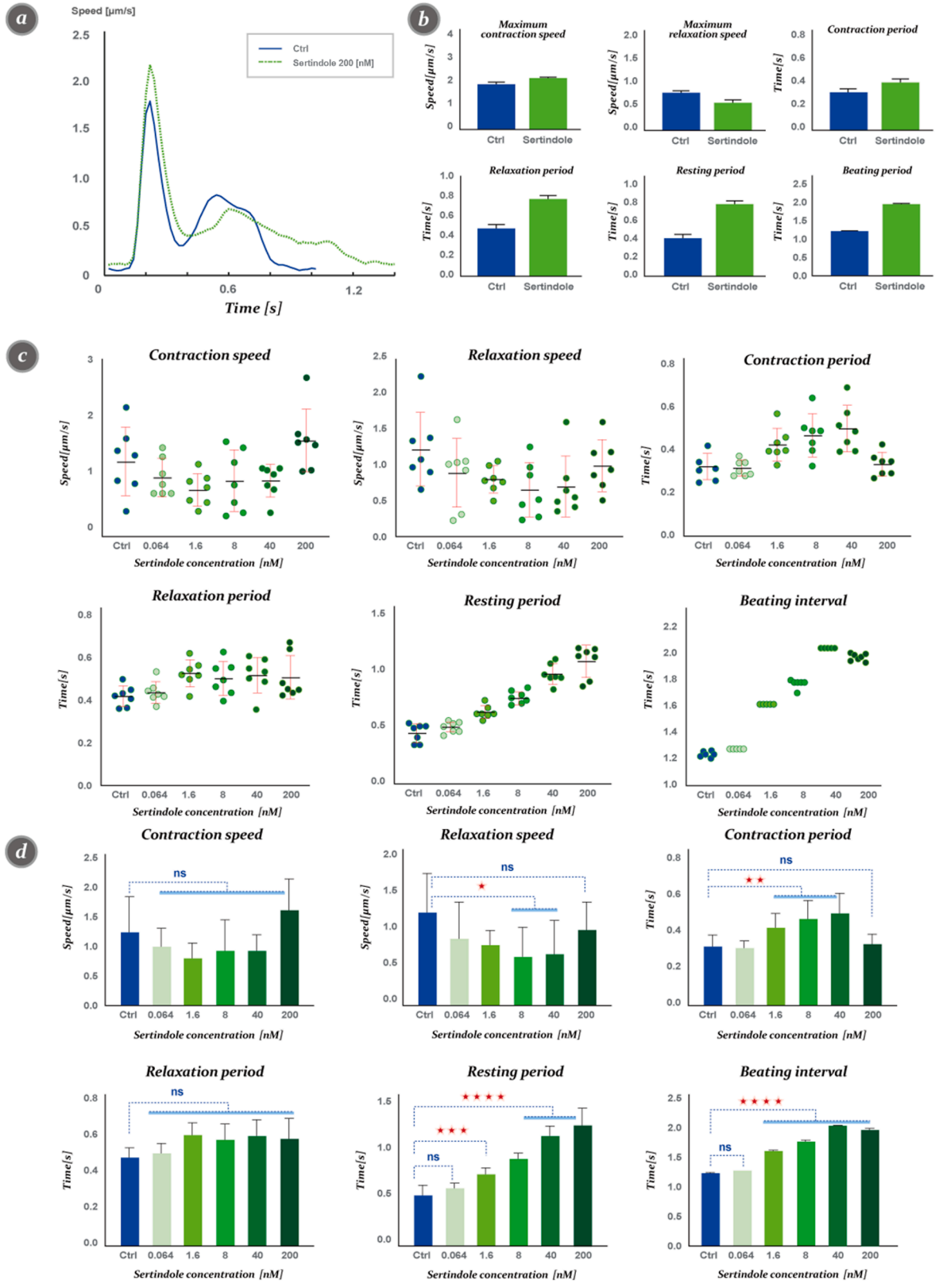


Fig. 2. Multiple parameter measurements for individually extracted cells in response to sertindole at different concentrations. (a) The representation of the action potential motion–speed evaluation of whole-slide QPIs in the presence of sertindole drug versus control conditions in response to 200 nM of sertindole (a single beat is shown). (b) The variations of the critical parameter of whole-slide QPIs expressed in terms of mean and SD for control and drug-treated conditions. (c) The effect of the drug corresponded to increases in concentrations, where each cell's behavior was separately investigated (see Supplementary Video 2). (d) the bar graph of the average population of single cells. The graph shows a summary of the changes in the mean and standard deviation. An unpaired *t*-test was performed to detect significant differences between averaged groups.

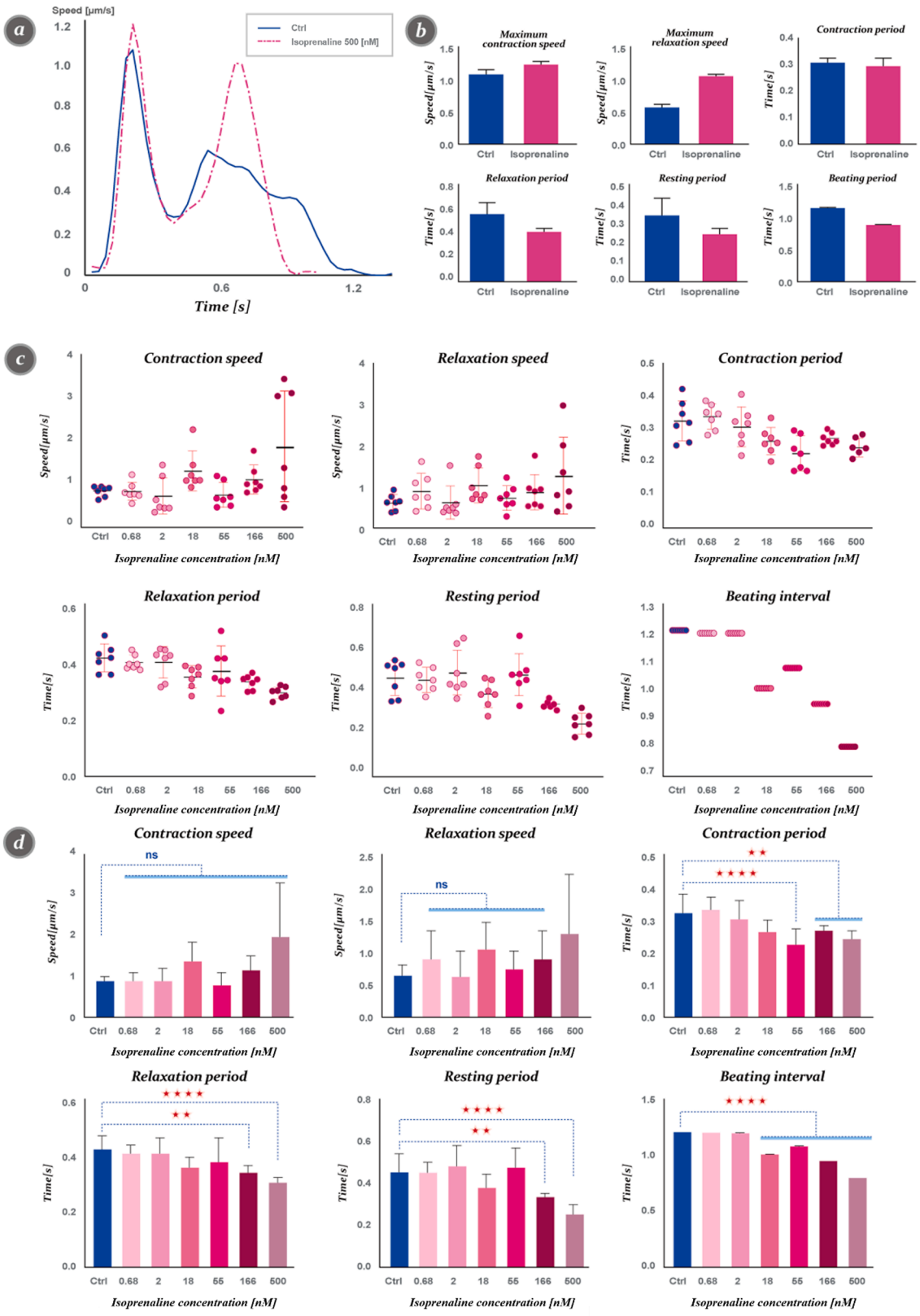


Fig. 3. Multiple parameter measurements per individually extracted cells treated with different concentrations of isoprenaline. (a) The representation of the action potential motion–speed evaluation of whole-slide QPIs in the presence of isoprenaline drug versus control conditions in response to 500 nM of isoprenaline (a single beat is shown). (b) The variations of the critical parameter of whole-slide QPIs are expressed in terms of mean and SD for control and drug-treated conditions. (c) The effect of the drug on each cell's behavior from increasing the concentration was investigated individually for the population of a single cell (see Supplementary Video 3). (d) The bar graph of the average population of single cells. The graph shows the changes in the mean and standard deviation of each quantification parameter calculated from the average of the single-cell population. An unpaired *t*-test was conducted to detect significant differences between averaged groups.

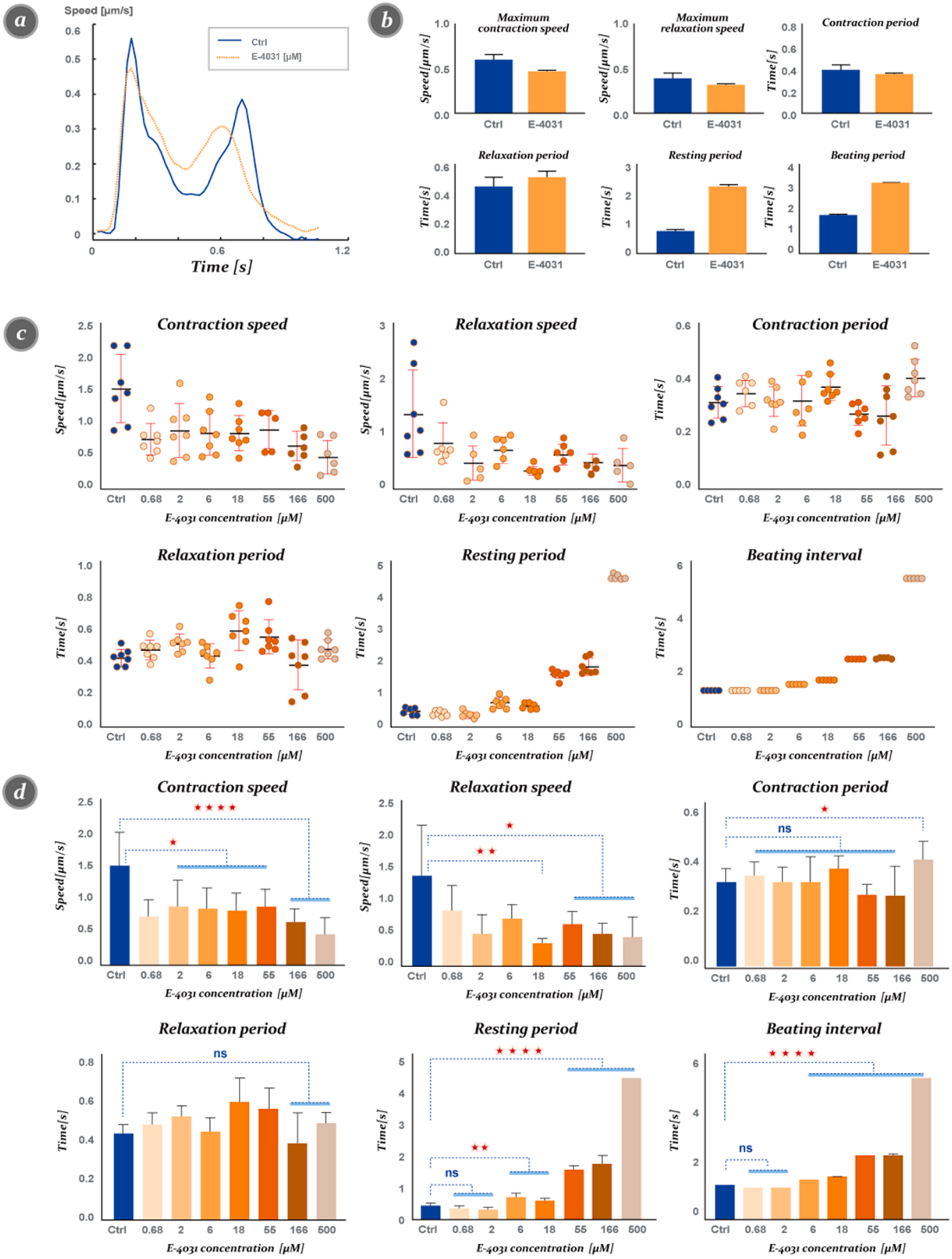


Fig. 4. Multiple parameter measurements per individually extracted cells treated with different concentrations of E-4031. (a) The representation of the action potential motion–speed evaluation of whole-slide QPIs in the presence of different drugs versus control conditions in response to 500 μM of E-4031 (a single beat is shown). (b) The variations of the critical parameter expressed in terms of mean and SD for control and drug-treated conditions of whole-slide QPIs. (c) The effect of different concentrations of E-4031 on each cardiomyocyte was individually investigated for every single cell (see Supplementary Video 4). (d) A bar graph for the average population of single cells shows a summary of the changes in mean and standard deviation as calculated from the average of the single-cell population. An unpaired *t*-test was conducted to detect significant differences between averaged groups.

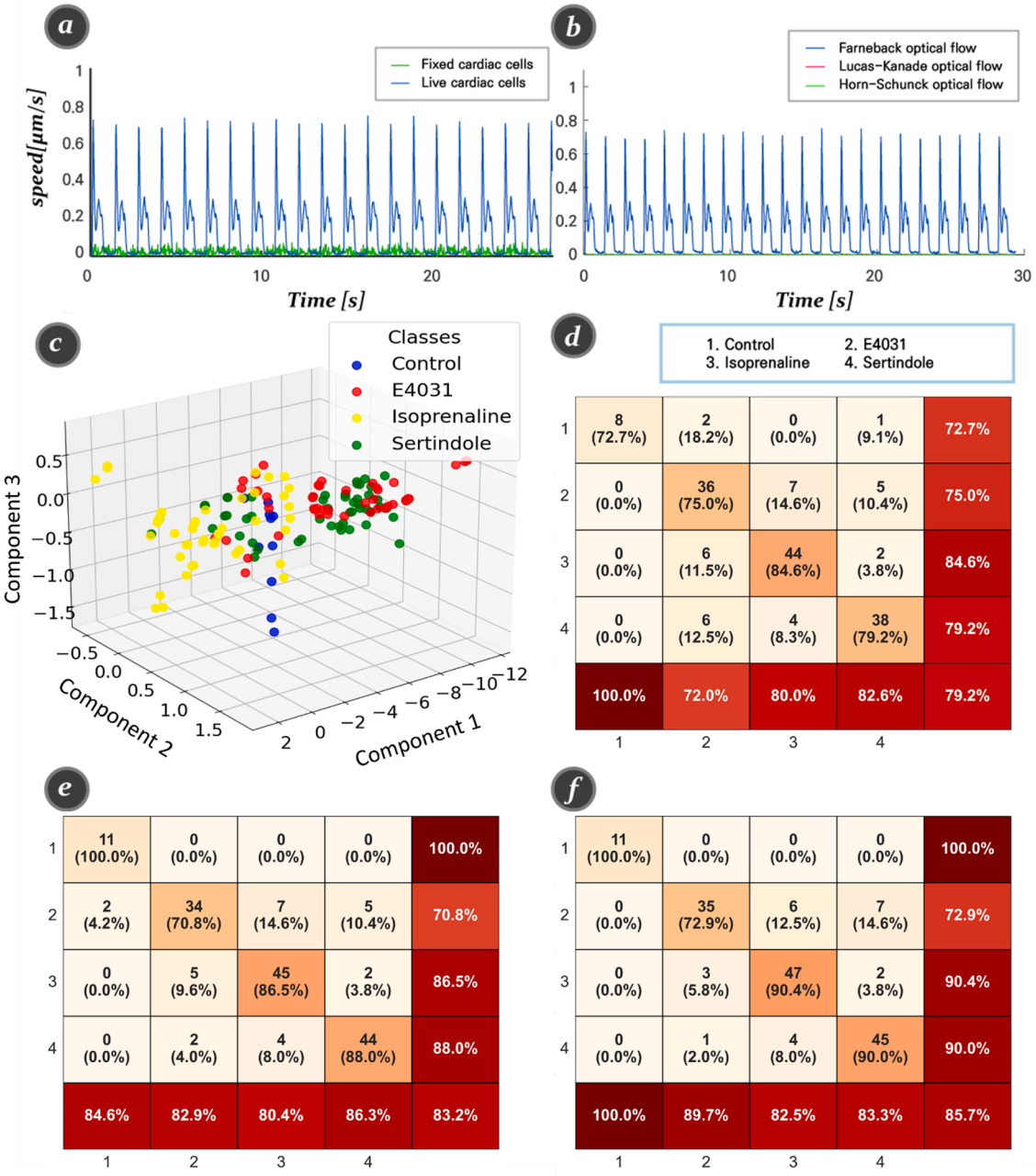


Fig. 5. Verification of proposed method and cardiac cells feature-based classification using machine learning-based approaches. (a) Beating profiles of whole-slide QPIs of multiple live cardiac cells under control conditions compared against fixed cardiac cells. (b) Comparison of different optical flow-based models for motion tracking of whole-slide QPIs of multiple cardiac cells under control conditions. (c) Original data distribution in 3D feature space using t-SNE, (d) confusion matrix of classification result using ANN, (e) confusion matrix of classification result using SVM model, (f) confusion matrix of classification result using KNN model.

testing in each iteration. To maintain proportional representation of all classes, stratified sampling was used, ensuring that each class's distribution was preserved in both training and test sets. The same training/test set division was consistently applied across all methods for a fair comparison of their performance. The data obtained from each single cell was assigned exclusively to either the training or test set to ensure that the two sets remained independent.

First, we used t-SNE to decrease the feature dimension to three features (3 components). Fig. 5(c) graphically depicts the original data distribution in 3D feature space, demonstrating that using the 3 components would result in complex and overlapped data distribution, which is challenging for feature-based classification using machine learning approaches. In this experiment, we used the seven primary characteristics collected from each cell, including (contraction-period, relaxation-period, contraction speed, relaxation speed, beating rate, beating intervals, and resting period). We utilized different machine-learning approaches, including the artificial neural network (ANN) [42], the support vector machine (SVM) [43], and the K-nearest neighbor (KNN) [44]. The suggested ANN model had three layers: an input layer, a hidden layer, and an output layer. The input layer consisted of seven neurons corresponding to the extracted seven features. The hidden layer also contained seven neurons, with a Rectified Linear Unit (ReLU) activation function applied to introduce non-linearity and improve model learning capability. The output layer comprised four neurons representing the number of classes. This architecture was chosen based on the complexity of the dataset and the need to achieve a balance between computational efficiency and classification performance. For the SVM model, we employed a kernel-based template using

a one-vs-one coding design for multi-class classification. Kernel-based learning was applied with the kernel scale set to auto, allowing the model to optimize feature scaling. Regularization parameter was set to auto, enabling the model to automatically balance margin maximization and error minimization. The number of expansion dimensions was set to auto, optimizing the feature space dimensionality. The training process was capped at 1000 iterations to ensure convergence. This configuration enabled effective multi-class classification while minimizing manual hyper-parameter tuning. For the KNN model, we implemented a subspace ensemble method with KNN learners, which were configured as follows. The number of neighbors was set to 3 for each learner, providing a balance between classification accuracy and computational

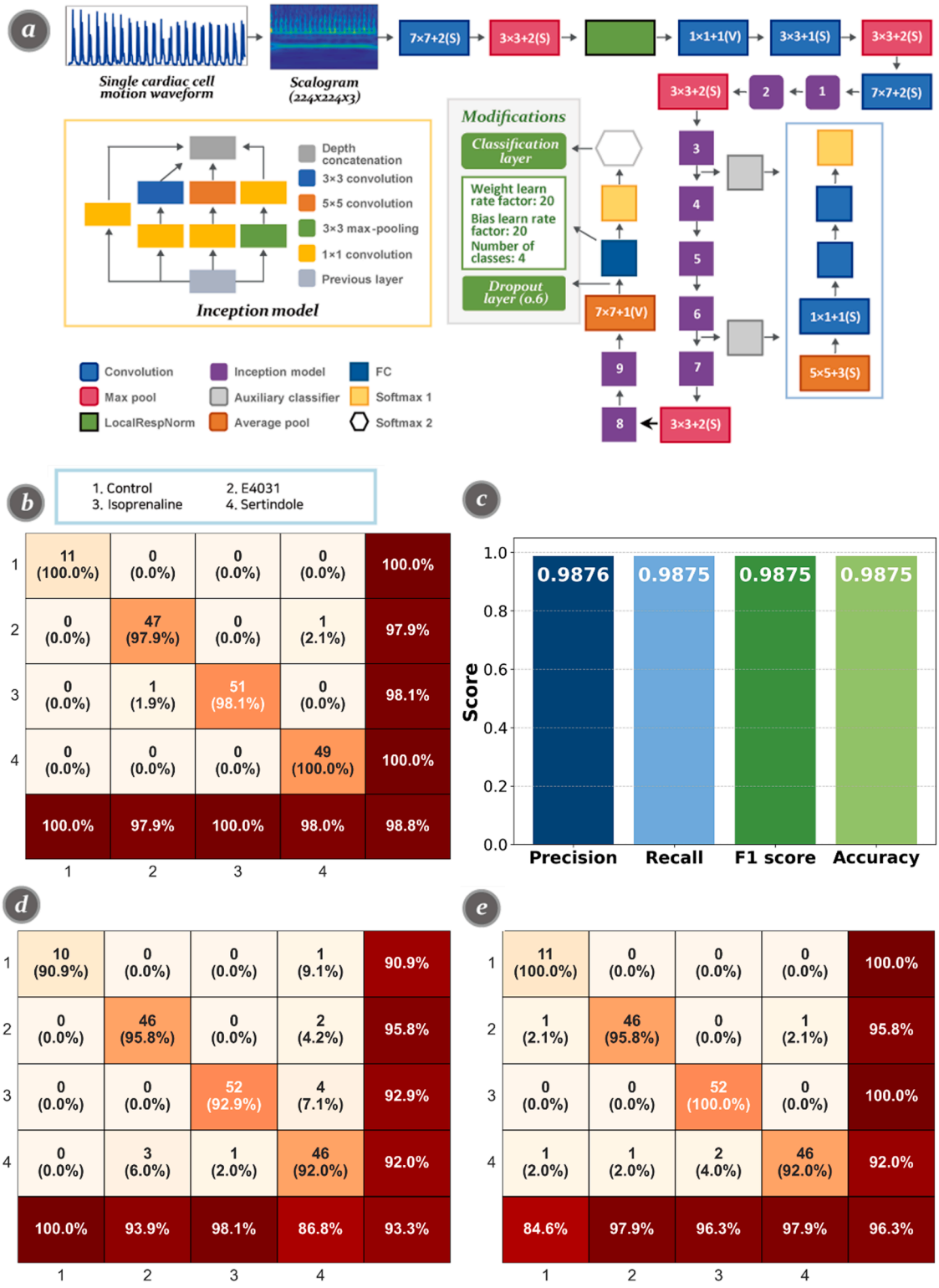


Fig. 6. Network performance from motion-based single cardiac–cell identification: (a) The overall structure of the modified GoogLeNet for single cardiac–cell motion waveform classification, (b) confusion matrix of the classification results with modified GoogLeNet, (c) experimental results from model performance using different evaluation metrics, (d) confusion matrix of the classification results with ResNet, and (e) confusion matrix of the classification results with DenseNet.

efficiency. Euclidean distance was used as the metric to measure similarity between data points, ensuring a straightforward and effective comparison. Uniform weighting was applied, meaning that all neighbors contributed equally to the classification decision. The confusion matrix of classification accuracy using the suggested ANN is shown in Fig. 5(d). Fig. 5(e) depicts the confusion matrix of classification accuracy of the SVM model. Fig. 5(f) depicts the confusion matrix of classification accuracy for KNN.

3.4. Drug identification using fine-tuned googlenet

The deep learning approach can perform automated feature extraction directly from the data without the need for manually engineered features. In the classification using deep learning, a total of 161 single cells were used, the same as in machine learning. There were 11 single cells in the control condition, 48 single cells for E-4031, 52 single cells for isoprenaline, and 50 single cells for the drug sertindole. We also performed 5-fold cross validation in the same way as machine learning. However, our dataset was quite small and computationally beneficial. Transfer learning is a promising approach that overcomes the above-mentioned limitations that uses a pre-trained, deep neural network. GoogLeNet is a deep CNN developed to classify the ImageNet database into 1000 classes after training with one million images. However, one can modify network layers to gain better results. We proposed a deep transfer learning-based approach using a modified GoogLeNet for automated drug identification from contractile motion waveforms. To train the modified GoogLeNet, we converted 1D single-cell motion waveforms into 2D images (scalograms) using continuous wavelet transform (CWT).

3.4.1. Continuous wavelet transform

CWT is used to construct a time-frequency representation of a signal that offers time and frequency localization. To make a one-dimensional signal into a 2D image (or scalogram) for CNN training, the CWT method was utilized. CWT plots the 1D signal as a function of time and frequency from estimations of similarity between the signal and an analysis function using an inner product, as seen in Eq. (6). For scale parameter $a > 0$ and position b, the CWT is:

$$c(a,b;f(t),\psi(t)) = \int_{-\infty}^{\infty} f(t)\frac{1}{a}\psi * \left(\frac{t-b}{a}\right)dt, \tag{6}$$

where ψ denotes the wavelet function, t stands for time and * indicates the complex conjugate. Continuously varying scale parameter value a and position b obtains CWT coefficients $c(a, b)$. The CWT coefficients are affected by the choice of wavelet, values of the scale, and position.

3.4.2. Image-based cardiac cell classification using deep learning approaches

GoogLeNet is a deep CNN model based on the inception architecture. The inception architecture piles these modules on each other, with an occasional max-pooling operation of stride 2×2 to reduce the input resolution (see Fig. 6(a)). However, depending on the special characteristics of our data, we added a drop-out layer (0.6) after the last fully connected layer to prevent network overfitting (see Fig. 6(a)). A dropout value of 0.6 was applied to prevent overfitting during training, as it is commonly used in similar studies and has been shown to be effective in balancing generalization and performance. To ensure the robustness of this choice, we conducted additional experiments with dropout values of 0.3, 0.5, and 0.7, which demonstrated no significant difference in model performance. Based on these results, we confirmed that the dropout value of 0.6 was suitable for our dataset and model architecture. The performance of the model was evaluated using a confusion matrix, which is a widely used method for measuring the accuracy of machine learning methods. The confusion matrix details are explained is in Supplementary Table 2. The results were compared against feature-based single cells classification using machine learning approaches (see Supplementary Table 3).

The confusion matrix from the fine-tuned GoogLeNet's performance identifies the different drugs from motion-beating activity (see Fig. 6 (b)). As shown, the confusion matrix's overall accuracy was 98.8 %. The classification performance metrics, including accuracy, precision, recall, and F1-measure (see Fig. 6(c)), were evaluated using a one-vs-all approach. In this method, each class was treated as the positive class while all other classes were treated as the negative class. The metrics were calculated for each class individually and averaged to provide a balanced evaluation of the classifier's performance across all classes. The equations for each metric are presented in equations (10), (11), (12), and (13) in Supplementary Section 4, respectively.

To validate our choice, we conducted a comparative analysis with other deep learning architectures, including ResNet and DenseNet. The evaluation results indicated that GoogLeNet achieved the highest classification accuracy, whereas ResNet and DenseNet achieved 93.3 % and 96.3 % (see Fig. 6(d) and (e)), respectively. While ResNet and DenseNet exhibited strong feature extraction capabilities, GoogLeNet outperformed them in terms of accuracy and computational efficiency, making it the most suitable choice for this study.

4. Discussion

The present study evaluated the contractile characteristics of single drug-treated cardiomyocytes by measuring changes in beating frequency, along with other comparable baseline parameters, from quantitative phase images that allow measuring hiPSC kinetic responses to drugs at the single-cell level that cannot be identified with ordinary methods. The effects of three drugs (sertindole, isoprenaline, and E-4031) at different concentrations were analyzed. Our experimental results with E-4031 and isoprenaline showed good agreement with previous studies. Isoprenaline caused an increase in contraction–relaxation motion–speed, whereas sertindole caused increases in only contraction motion–speed. By contrast, sertindole reduced the relaxation motion–-speed and significantly prolonged the relaxation period. E-4031 showed a decrease in contraction–relaxation motion–speed.

All drugs caused alterations in the resting period, thus changing the beating frequency. The goals of these experiments were not only to monitor the kinetics of single CMs but also to measure other critical parameters regarding the beating activity profile generated using contractile motion–speed measurement. Measured features from the contractile motion profile at the single-cell level included maximum contraction–relaxation motion–speed, contraction–relaxation period, beating period, and resting period. Among these, the beating frequency and contraction-relaxation motion speeds are the most critical. The beating frequency serves as a primary indicator of cardiomyocyte rhythm and its response to drug treatment, highlighting potential arrhythmic effects or cardiotoxicity. The contraction-relaxation motion speeds provide detailed insights into the mechanical and functional alterations of cardiomyocytes under various drug conditions, reflecting changes in cellular energy dynamics and overall contractile health. Together, these parameters allow a comprehensive assessment of the cardiomyocyte's physiological state and the drug's impact at the single-cell level.

Furthermore, we proposed a fine-tuned, deep transfer learning-based model for automated drug identification from a single-cell motion waveform. Performance analysis showed the proposed model achieved 98.8 % accuracy for automated drug type identification from a single cardiac cell motion waveform. The classification results using transfer learning were compared against feature-based classification results using different machine learning-based approaches. We showed that the current platform can be used to quantitatively predict potential cardiotoxicity from single-CM kinetics monitoring; it can be used to promote the maturation of in vitro hiPSCs and can reduce animal testing for cardiac safety screening.

The proposed method provides a promising tool for analyzing drug-induced effects on cardiomyocytes. To transition from academic research setting to an industrial application, several key steps are necessary, including scalability improvements, regulatory compliance, and extensive validation with larger datasets. Automation of data processing, collaboration with industry stakeholders, and optimization for production-ready hardware will be crucial for successful deployment. These steps will ensure that the proposed method meets the requirements of real-world applications in pharmaceutical and biomedical industries. Key stakeholders include pharmaceutical companies that can use this method for preclinical cardiotoxicity screening and drug development, biotechnology companies that can apply it for regenerative medicine and cell-based therapies, and academic and clinical research institutions that can utilize it to study cardiomyocyte behavior under various experimental conditions.

5. Conclusion

In this paper, we proposed an integrated platform for the motion characterization of single cardiomyocytes from holographic images by using a combination of deep learning and dense Farneback optical flow. First, we extracted multiple single cardiac cell dry masses using an FCN-based deep learning model from a whole-slide QPI, and we calculated the contractile motion–speed of beating cells to track the cell's contractile motion frame by frame through the extracted single CMs with single-pixel displacement detection using the dense Farneback optical flow method. We demonstrated the robustness of our proposed algorithm by comparison with other optical flow methods for CM motion tracking. Second, we developed a computational algorithm to quantify critical parameters regarding a CM's beating activity profile. Our experimental results with sertindole-treated CMs exhibited an increase in contraction motion–speed but a decline in relaxation motion–speed. The E-4031–treated cardiomyocytes showed a decrease in contraction–relaxation motion–speed while increasing the resting duration. Isoprenaline showed its effects by increasing contraction–relaxation motion–speed and resulted in a decrease in the resting period. We also provided reliable synchronization analysis of drug-treated CMs owing to cellular analysis at the single-cell level. Third, we proposed a fine-tuned, deep transfer learning-based model for automated drug type identification from single-cell motion waveforms, achieving 98.8 % accuracy, and compared the results with feature-based classification using different machine learning-based methods.

The currently proposed method is a supervised classification method meaning that we need labeled data to train the model while it might not be always possible to have enough labeled data in medical image cases. In the future, we are planning to utilize unsupervised learning or a few-shot learning method that needs a few labeled data for training.

Ethics statement

This study complies with ethical standards. All data were sourced ethically or generated by the authors.

Supporting information

Supporting document is provided for this work. Figure S1: (a) Diagram of off-axis digital holographic microscopy used to acquire cardiomyocyte images(a) Diagram of off-axis digital holographic microscopy used to acquire cardiomyocyte images. (b) A recorded hologram of a control cardiomyocyte sample (the inset shows a three-dimensional portion of the hologram. (c) The spectrum of the off-axis hologram (three bandwidths are isolated). (d) Spatial filtering can preserve the bandwidth of the real image. (e) Amplitude image after numerical reconstruction. (f) Phase image after numerical reconstruction and phase unwrapping. The phase image provides high-contrast data for quantitative analysis. Figure S2: Multi-resolution leveling of the image, and the optical flow method for pixel motion detection. (a) Multi-resolution leveling of the image with three levels. The image resolution at each level is downsized. The tracking begins at the lowest level and finishes at the highest. (b) A representation of the optical flow method for pixel displacement estimation. Black pixels correspond to the pixel position at time t, and yellow pixels correspond to the pixel position at time $t + \mathrm{dt}$. Figure S3: Beat rate profiles of whole-slide QPIs for multiple cardiac cells under control conditions and treated with E-4031, isoprenaline, and sertindole. Figure S4: The beat rates before and after applying the drugs at different concentrations. An image sequence for the control condition was recorded before drug treatment. Afterward, the sample was treated with a specific drug concentration. After incubation (15 min), beats per minute (BPM) was measured again. Figure S5: Critical parameter measurement of whole slide QPI of multiple cardiac cells treated with different concentrations of Sertindole compound. Figure S6: Critical parameter measurement of whole slide QPI of multiple cardiac cells treated with different concentrations of E-4031 compound. Figure S7: Critical parameter measurement of whole slide QPI of multiple cardiac cells treated with different concentrations of Isoprenaline compound. Figure S8: Synchronization analysis of single cardiac cells. (a) rhythm strip comparison of single cardiac cells under control conditions (b) cross-correlation analysis between different pairs of single cardiac cells under control conditions. (c),(d) rhythm strip comparison of single cells E-4031 drug 500 μM and cross-correlation analysis between single pairs of cells respectively. Figure S9: Synchronization analysis of single cardiac cells. (a),(b) rhythm strip comparison of single cells Isoprenaline drug 500 nM and cross-correlation analysis between single pairs of cells respectively. (c),(d) rhythm strip comparison of single cells sertindole drug 200 nM and cross-correlation analysis between single pairs of cells respectively. Table 1: Quantitative parameters and descriptions were measured from whole-slide QPI of cardiomyocytes from control samples. Table 2: Confusion matrix of evaluation measures from the classification results. Table 3 Classification accuracy result of the proposed transfer learning-based model based on motion waveform comparison against feature-based classification using machine learning approaches. Video 1: The motion–speed beating activity profile of a single CM using the cell's motion–speed measurement. Video 2: The effect of the Sertindole drug where each cell's behavior was separately investigated. Video 3: The effect of the Isoprenaline drug where each cell's behavior was separately investigated. Video 4: The effect of the E-4031 drug where each cell's behavior was separately investigated. Video 5: Verification of the proposed method by beating activity profile measurement of the fixed cardiac cell using the proposed method.

CRediT authorship contribution statement

Ezat Ahmadzadeh: Methodology, Writing – original draft. **Seonghwan Park:** Methodology, Writing – original draft. **Youhyun Kim:** Validation, Writing – review & editing. **Inkyu Moon:** Conceptualization, Funding acquisition, Methodology, Supervision, Writing – review & editing.

Declaration of competing interest

The authors declare that they have no known competing financial interests or personal relationships that could have appeared to influence the work reported in this paper.

Acknowledgments

This work was supported by the National Research Foundation of Korea (NRF) grant funded by the Korea government (MSIT) (RS-2023–00253613). The authors thank Dr. Benjamin Rappaz and Prof. Gerardo Turcatti (BSF in EPFL, Lausanne, Switzerland) for helpful discussion and providing the datasets.

Supplementary materials

Supplementary material associated with this article can be found, in the online version, at doi:10.1016/j.cmpb.2025.108890.

References

[1] D. Carl, B. Kemper, G. Wernicke, G. Von Bally, Parameter-optimized digital holographic microscope for high-resolution living-cell analysis, Appl. Opt. 43 (2004) 6536–6544.

[2] J. Kühn, E. Shaffer, J. Mena, B. Breton, J. Parent, B. Rappaz, M. Chambon, Y. Emery, P. Magistretti, C. Depeursinge, P. Marquet, G. Turcatti, Label-free cytotoxicity screening assay by digital holographic microscopy, Assay. Drug Dev. Technol. 11 (2013) 101–107.

[3] E. Matsa, P.W. Burridge, J.C. Wu, Human stem cells for modeling heart disease and for drug discovery, Sci. Transl. Med. 6 (2014) 239ps6.

[4] T. Wang, N. Hu, J. Cao, J. Wu, K. Su, P. Wang, A cardiomyocyte-based biosensor for antiarrhythmic drug evaluation by simultaneously monitoring cell growth and beating, Biosens. Bioelectron. 49 (2013) 9–13.

[5] I. Moon, M. Daneshpanah, B. Javidi, A. Stern, Automated three-dimensional identification and tracking of micro/nanobiological organisms by computational holographic microscopy, Proc. IEEE 97 (2009) 990–1010.

[6] B. Rappaz, I. Moon, F. Yi, B. Javidi, P. Marquet, G. Turcatti, Automated multi-parameter measurement of cardiomyocytes dynamics with digital holographic microscopy, Opt. Express. 23 (2015) 13333–13347.

[7] N.T. Shaked, L.L. Satterwhite, N. Bursac, A. Wax, Whole-cell-analysis of live cardiomyocytes using wide-field interferometric phase microscopy, Biomed. Opt. Express. 1 (2010) 706–719.

[8] S.L. Zhang, L. Liu, S. Ren, Z.I. Li, Y.H. Zhao, Z.G. Yang, R. Hu, J.L. Qu, Recent advances in nonlinear optics for bio- aging applications, Opto-Electron. Adv. 3 (2020) 200003.

[9] B. Rappaz, E. Cano, T. Colomb, J. Kühn, C. Depeursinge, V. Simanis, P. J. Magistretti, P. Marquet, Noninvasive characterization of the fission yeast cell cycle by monitoring dry mass with digital holographic microscopy, J. Biomed. Opt. 14 (2009) 034049.

[10] I. Moon, E. Ahmadzadeh, K. Jaferzadeh, N. Kim, Automated quantification study of human cardiomyocyte synchronization using holographic imaging, Biomed. Opt. Express. 10 (2019) 610–621.

[11] J. Chu, W. Dong, Z. Huang, Endpoint prediction of heart failure using electronic health records, J. Biomed. Inf. 109 (2020) 103518.

[12] I. Moon, K. Jaferzadeh, E. Ahmadzadeh, B. Javidi, Automated quantitative analysis of multiple cardiomyocytes at the single-cell level with three-dimensional holographic imaging informatics, J. Biophotonics. 11 (2018) e201800116.

[13] A. Brüggemann, C. Haarmann, M. Rapedius, T. Goetze, I. Rinke, M. George, N. Fertig, Characterization of iPS derived cardiomyocytes in voltage clamp and current clamp by automated patch clamp, Biophys. J. 112 (2017) 236a.

[14] D. Ossola, M.-Y. Amarouch, P. Behr, J. Vörös, H. Abriel, T. Zambelli, Force-controlled patch clamp of beating cardiac cells, Nano Lett. 15 (2015) 1743–1750.

[15] G.T. Dempsey, K.W. Chaudhary, N. Atwater, C. Nguyen, B.S. Brown, J.D. McNeish, A.E. Cohen, J.M. Kralj, Cardiotoxicity screening with simultaneous optogenetic pacing, voltage imaging and calcium imaging, J. Pharmacol. Toxicol. Methods 81 (2016) 240–250.

[16] E. Grespan, S. Martewicz, E. Serena, V. Le Houerou, J. Rühe, N. Elvassore, Analysis of calcium transients and uniaxial contraction force in single human embryonic stem cell-derived cardiomyocytes on microstructured elastic substrate with spatially controlled surface chemistries, Langmuir 32 (2016) 12190–12201.

[17] C. Bazan, D. Torres Barba, P. Blomgren, P. Paolini, Image processing techniques for assessing contractility in isolated neonatal cardiac myocytes, Int. J. Biomed. ImAging (2011) 729732.

[18] T. Hayakawa, T. Kunihiro, T. Ando, S. Kobayashi, E. Matsui, H. Yada, Y. Kanda, J. Kurokawa, T. Furukawa, Image-based evaluation of contraction-relaxation kinetics of human-induced pluripotent stem cell-derived cardiomyocytes: correlation and complementarity with extracellular electrophysiology, J. Mol. Cell Cardiol. 77 (2014) 178–191.

[19] R. Chandrashekara, A. Rao, G.I. Sanchez-Ortiz, R.H. Mohiaddin, D. Rueckert, Construction of a statistical model for cardiac motion analysis using nonrigid image registration, in: C. Taylor, J.A. Noble (Eds.), Information Processing in Medical Imaging. IPMI 2003. Lecture Notes in Computer Science, Information Processing in Medical Imaging. IPMI 2003. Lecture Notes in Computer Science, vol 2732, Springer, Berlin, Heidelberg, 2003, pp. 599–610.

[20] M. Salvador, F. Regazzoni, A. Quarteroni, Fast and robust parameter estimation with uncertainty quantification for the cardiac function, Comp. Meth. Progr. Biomed. 231 (2023) 107402.

[21] J.-Q He, Y. Ma, Y. Lee, J.A. Thomson, T.J. Kamp, Human embryonic stem cells develop into multiple types of cardiac myocytes: action potential characterization, Circ. Res. 93 (2003) 32–39.

[22] P. Hoang, N. Huebsch, S.H. Bang, B.A. Siemons, B.R. Conklin, K.E. Healy, Z. Ma, S. Jacquir, Quantitatively characterizing drug-induced arrhythmic contractile motions of human stem cell-derived cardiomyocytes, Biotechnol. Bioeng. 115 (2018) 1958–1970.

[23] M. Maddah, J.D. Heidmann, M.A. Mandegar, C.D. Walker, S. Bolouki, B.R. Conklin, K.E. Loewke, A non-invasive platform for functional characterization of stem-cell-derived cardiomyocytes with applications in cardiotoxicity testing, Stem. Cell Rep. 4 (2015) 621–631.

[24] E. Ahamadzadeh, K. Jaferzadeh, S. Park, S. Son, I. Moon, Automated analysis of human cardiomyocytes dynamics with holographic image-based tracking for cardiotoxicity screening, Biosens. Bioelectron. 195 (2022) 113570.

[25] L.-C Chen, P. Bentley, K. Mori, K. Misawa, M. Fujiwara, D. Rueckert, DRINet for medical image segmentation, IEEe Trans. Med. ImAging 37 (2018) 2453–2462.

[26] L.-C Chen, G. Papandreou, I. Kokkinos, K. Murphy, A.L. Yuille, DeepLab: semantic image segmentation with deep convolutional nets, atrous convolution, and fully connected CRFs, IEEe Trans. Pattern. Anal. Mach. Intell. 40 (2018) 834–848.

[27] E. Rho, M. Kim, S.H. Cho, B. Choi, H. Park, H. Jang, Y.S. Jung, S. Jo, Separation-free bacterial identification in arbitrary media via deep neural network-based SERS analysis, Biosens. Bioelectron. (2022) 113991.

[28] Z. Yan, Y. Su, H. Sun, H. Yu, W. Ma, H. Chi, H. Cao, Q. Chang, SegNet-based left ventricular MRI segmentation for the diagnosis of cardiac hypertrophy and myocardial infarction, Comp. Meth. Progr. Biomed. 227 (2022) 107197.

[29] E. Ahmadzadeh, K. Jaferzadeh, S. Shin, I. Moon, Automated single cardiomyocyte characterization by nucleus extraction from dynamic holographic images using a fully convolutional neural network, Biomed. Opt. Express. 11 (2020) 1501–1516.

[30] E. Cuche, P. Marquet, C. Depeursinge, Simultaneous amplitude-contrast and quantitative phase-contrast microscopy by numerical reconstruction of Fresnel off-axis holograms, Appl. Opt. 38 (1999) 6994–7001.

[31] P. Marquet, B. Rappaz, P.J. Magistretti, E. Cuche, Y. Emery, T. Colomb, C. Depeursinge, Digital holographic microscopy: a noninvasive contrast imaging technique allowing quantitative visualization of living cells with subwavelength axial accuracy, Opt. Lett. 30 (2005) 468–470.

[32] K. Jaferzadeh, B. Rappaz, F. Kuttler, B.K. Kim, I. Moon, P. Marquet, G. Turcatti, Marker-free automatic quantification of drug-treated cardiomyocytes with digital holographic imaging, ACS. Photonics. 7 (2020) 105–113.

[33] G. Farnebäck, Two-frame motion estimation based on polynomial expansion, in: J. Bigun, T. Gustavsson (Eds.), Image Analysis. SCIA 2003. Lecture Notes in Computer Science, Image Analysis. SCIA 2003. Lecture Notes in Computer Science, vol 2749, Springer, Berlin, Heidelberg, 2003, pp. 363–370.

[34] I. Gandin, A. Scagnetto, S. Romani, G. Barbati, Interpretability of time-series deep learning models: a study in cardiovascular patients admitted to Intensive care unit, J. Biomed. Inf. 121 (2021) 103876.

[35] N.M. Arzeno, Z.-D. Deng, C.-S. Poon, Analysis of first-derivative based QRS detection algorithms, IEEE Trans. Biomed. Eng. 55 (2008) 478–484.

[36] A. Ruha, S. Sallinen, S. Nissilä, A real-time microprocessor QRS detector system with a 1-ms timing accuracy for the measurement of ambulatory HRV, IEEE Trans. Biomed. Eng. 44 (1997) 159–167.

[37] O. Mutlu, G. Ulak, I.K. Celikyurt, F.Y. Akar, F. Erden, Effects of olanzapine, sertindole and clozapine on learning and memory in the Morris water maze test in naive and MK-801-treated mice, Pharmacol. Biochem. Behav. 98 (2011) 398–404.

[38] C. Luo, K. Wang, H. Zhang, Modelling the effects of quinidine, disopyramide, and E-4031 on short QT syndrome variant 3 in the human ventricles, Physiol. Meas. 38 (2017) 1859–1873.

[39] S.J. Roy, P.S. Mainzen Prince, Protective effects of sinapic acid on cardiac hypertrophy, dyslipidaemia and altered electrocardiogram in isoproterenol-induced myocardial infarcted rats, Eur. J. Pharmacol. 699 (2013) 213–218.

[40] J. Guo, C. Zhu, Dynamic displacement measurement of large-scale structures based on the Lucas–Kanade template tracking algorithm, Mech. Syst. Signal. Process. 66–67 (2016) 425–436.

[41] X. Gong, S. Bansmer, Horn–Schunck optical flow applied to deformation measurement of a birdlike airfoil, Chin. J. Aeronaut 28 (2015) 1305–1315.

[42] O.I. Abiodun, A. Jantan, A.E. Omolara, K.V. Dada, N.A.E. Mohamed, H. Arshad, State-of-the-art in artificial neural network applications, Heliyon 4 (2018) e00938.

[43] K.M. Lin, C.J. Lin, A study on reduced support vector machines, IEEe Trans. Neural Netw. 14 (2003) 1449–1459.

[44] Y. Zhang, G. Cao, B. Wang, X. Li, A novel ensemble method for k-nearest neighbor, Pattern. Recognit. 85 (2019) 13–25.